

SIMULATION OF STOCHASTIC REACTION-DIFFUSION PROCESSES ON UNSTRUCTURED MESHES

STEFAN ENGBLOM¹, LARS FERM¹
ANDREAS HELLANDER¹, PER LÖTSTEDT¹ *

October 30, 2018

¹*Division of Scientific Computing, Department of Information Technology
Uppsala University, P. O. Box 337, SE-75105 Uppsala, Sweden
emails: stefane, ferm, andreas.hellander, perl@it.uu.se*

Abstract

Stochastic chemical systems with diffusion are modeled with a reaction-diffusion master equation. On a macroscopic level, the governing equation is a reaction-diffusion equation for the averages of the chemical species. On a mesoscopic level, the master equation for a well stirred chemical system is combined with Brownian motion in space to obtain the reaction-diffusion master equation. The space is covered by an unstructured mesh and the diffusion coefficients on the mesoscale are obtained from a finite element discretization of the Laplace operator on the macroscale. The resulting method is a flexible hybrid algorithm in that the diffusion can be handled either on the meso- or on the macroscale level. The accuracy and the efficiency of the method are illustrated in three numerical examples inspired by molecular biology.

Keywords: master equation, diffusion, reaction rate equations, hybrid method, finite element method, unstructured mesh.

AMS subject classification: 65C40, 65C05, 65M60, 60H35.

*Financial support has been obtained from the Swedish Foundation for Strategic Research and the Swedish National Graduate School in Mathematics and Computing. Corresponding author: Per Lötstedt, address as above, telephone +46-18-4712972, fax +46-18-523049.

Abbreviations

Abbreviation	Expanded form
mRNA	messenger ribonucleic acid
CME	chemical master equation
PDF	probability density function
SSA	stochastic simulation algorithm
RRE	reaction rate equations
ODE	ordinary differential equation
RDME	reaction-diffusion master equation
NRM	next reaction method
NSM	next subvolume method
BD	Brownian dynamics
PDE	partial differential equation
RDE	reaction-diffusion equation
nD	n space dimensions
FEM	finite element method
SPDE	stochastic PDE
FVM	finite volume method

Table 0.1: Abbreviations in the paper in order of appearance.

1 Introduction

Intrinsic noise in biochemical networks can have a large impact on the macroscopic behavior of biological cells [11, 29, 32, 36, 38]. An example is the regulation of the transcription of genes to messenger RNA (mRNA) where genes are present in one or two copies and the copy number of mRNA is small. The facts that the copy number is a small nonnegative integer and that there is a probability that a certain reaction will occur when two molecules meet make a discrete, stochastic description of the system necessary.

The state of the system is the number of molecules of each participating species. Usually, the assumption is that the system is well stirred such that there is no spatial dependence of the distribution of the chemical species. Then the chemical master equation (CME) is the governing equation for the probability density function (PDF) of the state of the chemical system [16, 27]. A trajectory of the biochemical system is simulated by randomly choosing a reaction and then updating the state vector in Gillespie’s Stochastic Simulation Algorithm (SSA) [19], further developed in [6, 9, 18, 22] to improve the efficiency and to handle systems with slow and fast time scales. The concentrations of the species at a macroscopic level are often approximated by the reaction rate equations

(RRE) which is a deterministic system of nonlinear ordinary differential equations (ODEs). This approach works well only when the number of molecules is large, a condition which is often violated inside living cells [21].

There are many biochemical systems where the spatial inhomogeneity of the species cannot be neglected. Such systems are no longer well stirred since the transport of the molecules through the solvent is slow compared to typical reaction times [28] or since some reactions are strongly localized. The correlation length, i.e. the length scale on which the system can be regarded as spatially homogeneous, is now much shorter. Examples are found in [7, 8, 10, 14, 33] where both the stochastic properties and the spatial distribution are necessary to explain experimental data. If the diffusion at a molecular level is treated as a special set of reactions in the CME, then we arrive at the reaction-diffusion master equation (RDME) [16, Ch. 8], [27, Ch. XIV], [30]. This is an equation for the time evolution of the PDF of the state of the system in the same manner as the CME but the dimensionality of the problem is much higher.

In the RDME, the geometry is partitioned into computational cells and in each cell there is a stochastic variable representing the number of molecules of each species. If the number of species is N and the number of cells is K then the RDME is an equation for the scalar PDF in KN dimensions and time. For example, for a small problem with five species and 100 nodes in a mesh, the dimensionality is 500 and a direct solution of the RDME is obviously out of the question. The only feasible way is to generate samples from the RDME and collect statistics in a Monte Carlo fashion. Examples where the SSA has been applied to reaction-diffusion systems in one space dimension can be found in [3, 42]. An efficient version of the SSA is the *next reaction method* (NRM) [18]. An implementation of the NRM, specially developed for diffusive systems, is the *next subvolume method* (NSM) [10], implemented in the freely available computer software MesoRD [23].

More accurate modeling may be necessary if the number of molecules is very low. In Brownian dynamics (BD), the separate paths of single molecules are tracked and they may react with other molecules in their vicinity [1, 39, 47]. The reaction and diffusion of the particles are simulated using the Green's function of the Smoluchowski and diffusion equation in [47]. The BD approach is possible only if the total number of molecules is small and becomes inefficient when there are many nonreactive collisions for each reactive one. The RDME and BD are compared in [7].

The corresponding macroscopic equation for the concentrations of the species is a partial differential equation (PDE): the reaction-diffusion equation (RDE). This is the equation solved in applications such as combustion [37] and the model is appropriate when the number of molecules is large and stochastic effects can be neglected.

In this paper, we develop a method for simulating the RDME on an unstructured mesh consisting of triangles in two space dimensions (2D) or tetrahedra in

3D. Unstructured meshes have the advantage of approximating curved inner and outer boundaries much more accurately than Cartesian meshes do. The diffusion coefficients at the meso level are chosen to be consistent with the discretization with the finite element method (FEM) on the mesh converging to the diffusion operator at the macro level when the cell size vanishes. With a proper computational mesh [17], the FEM approximation yields positive probabilities for a particle to jump into the adjacent cell. The time integration of the RDME is split according to Strang [41] into two parts in a hybrid method: the diffusion and the chemical reactions. First, a macroscopic diffusive step is taken for a subset of the species with the diffusion operator at the macro level using the unstructured primal mesh. Then the stochastic reactions and the stochastic diffusion for the remaining species are advanced in the dual cells of the mesh with SSA at the meso level. If all species in all cells are treated at the meso level, then we exactly sample the RDME.

Hybrid methods for a well stirred system with a mesoscopic-macroscopic approximation are found in [22, 24]. In [34], an efficient Monte Carlo method for the diffusion equation is described. In [26], the mesoscopic diffusion coefficients are derived from the discretization of the Laplacian on a 2D Cartesian mesh with an interior boundary. With unstructured meshes, we propose in this paper to obtain those coefficients from a proper FEM discretization.

The outline of the paper is as follows. In Section 2, the RDME is stated and the relation to the RDE is discussed. The diffusion coefficients are derived from the discrete Laplacian in Section 3. The first and second moments of the distribution of molecules in a system without chemical reactions are derived in Section 4. The hybrid method coupling the meso- and macroscales and the operator splitting in time are found in Section 5. Three examples in 2D are found in the section with numerical results. It is shown that the suggested mesoscopic diffusion yields trajectories converging to the macroscopic diffusion equation. It is also shown that the hybrid method we propose accurately samples the RDME at a fraction of the time needed for a full simulation. Conclusions are drawn in the final section.

2 Reaction-Diffusion Master Equation

Assume that the computational domain Ω in space is partitioned into computational cells \mathcal{C}_j , $j = 1, \dots, K$, such that the cells do not overlap and they cover the whole domain

$$\mathcal{C}_i \cap \mathcal{C}_j = \emptyset, i \neq j, \quad \text{and} \quad \cup_{j=1}^K \mathcal{C}_j = \Omega.$$

Furthermore, assume that there are N chemically active species X_{ij} , $i = 1, \dots, N$, in the K cells, $j = 1, \dots, K$. The state of the system is the array \mathbf{x} with $N \times K$ components x_{ij} . The j th column of \mathbf{x} is denoted by $\mathbf{x}_{\cdot j}$ and the i th row by $\mathbf{x}_{i \cdot}$.

The non-negative integer x_{ij} is thus the copy number of species i in cell j . The time dependent state is changed by chemical reactions occurring between the molecules in the same cell and by diffusion where molecules move to adjacent cells. In the reactions, the species interact vertically in the array \mathbf{x} and in the diffusion, the interaction is horizontal. The RDME governs the time evolution of the PDF p , where $p(\mathbf{x}, t)$ is the probability to be in state \mathbf{x} at time t .

2.1 Chemical reactions

A reaction r in a cell j is a transition from one state $\tilde{\mathbf{x}}_{.j}$ before the reaction to the state $\mathbf{x}_{.j} = \tilde{\mathbf{x}}_{.j} - \mathbf{n}_r$ after the reaction. The state-change vector \mathbf{n}_r of a reaction is a vector with small integer numbers of length N independent of j . There is a reaction probability or *propensity* w_r that reaction r will take place in a cell depending on the state $\tilde{\mathbf{x}}_{.j}$. A chemical reaction in cell j can be written



In a system without diffusion, the PDF for the molecular distribution in \mathcal{C}_j satisfies the CME. Let \mathbf{n}_r be split into two parts

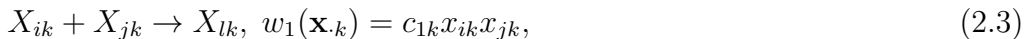
$$\mathbf{n}_r = \mathbf{n}_r^+ + \mathbf{n}_r^-, \quad n_{ri}^+ = \max(n_{ri}, 0), \quad n_{ri}^- = \min(n_{ri}, 0).$$

Then the CME for p is, see [16, Ch. 7], [27, Ch. V],

$$\begin{aligned} \frac{\partial p(\mathbf{x}, t)}{\partial t} = \mathcal{M}p(\mathbf{x}, t) \equiv & \quad (2.2) \\ & \sum_{j=1}^K \sum_{\substack{r=1 \\ \mathbf{x}_{.j} + \mathbf{n}_r^- \geq 0}}^R w_r(\mathbf{x}_{.j} + \mathbf{n}_r) p(\mathbf{x}_{.1}, \dots, \mathbf{x}_{.j} + \mathbf{n}_r, \dots, \mathbf{x}_{.K}, t) \\ & - \sum_{j=1}^K \sum_{\substack{r=1 \\ \mathbf{x}_{.j} - \mathbf{n}_r^+ \geq 0}}^R w_r(\mathbf{x}_{.j}) p(\mathbf{x}, t), \end{aligned}$$

where the constraints on \mathbf{x} are defined elementwise. These constraints are introduced in order to avoid unfeasible reactions and will be dropped in the following as is customary.

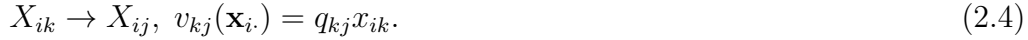
A simple reaction in \mathcal{C}_k is



where conventionally, we use uppercase letters to denote molecule *names*, while lowercases are used for counting the number of molecules of a certain species. The transition vector \mathbf{n}_1 is zero except for three components: $n_{1i} = n_{1j} = 1, n_{1l} = -1$. The propensity w_1 has the same form for all cells k , whereas the reaction coefficient c_{1k} scales with the area or volume $|\mathcal{C}_k|$ of the cell such that $c_{1k} = \hat{c}_1/|\mathcal{C}_k|$, where \hat{c}_1 is a constant.

2.2 Diffusion

Suppose now that there are no chemical reactions but only diffusion in the system. Then the mesoscale model of the diffusion of species i from one cell \mathcal{C}_k to another cell \mathcal{C}_j can be written as a chemical reaction (cf. (2.3))



It is understood that q_{kj} is non-zero only for those cells that are connected and $q_{jj} = 0$. The form of the propensity v_{kj} and the diffusion coefficient q_{kj} are the same for all species here but q_{kj} may depend on i and can be different for small and large molecules. We can write

$$q_{kj} = \gamma \frac{\hat{q}_{kj}}{h_{kj}^2}, \quad (2.5)$$

where γ is the macroscopic diffusion constant, h_{kj} is a measure of the local length-scale and \hat{q}_{kj} is dimensionless but still depends on the precise shapes of the cells \mathcal{C}_k and \mathcal{C}_j . The interpretation of q_{kj} as the inverse of the expected value of the *first exit time* for a single molecule from cell \mathcal{C}_k to \mathcal{C}_j makes it clear why no simple formula exists except for very regular cells. The molecular movement is often modeled by the Itô-diffusion

$$d\xi = \sigma dW_t, \quad (2.6)$$

where $\xi(t)$ is the position and W_t is a Wiener-process. The relation between γ in (2.5) and σ in (2.6) is then simply $\gamma = \sigma^2/2$.

With this notation, the master equation for the diffusion in (2.4) can be written in the same manner as the CME in (2.2), see [16, Ch. 8], [27, Ch. XIV], [30],

$$\begin{aligned} \frac{\partial p(\mathbf{x}, t)}{\partial t} = & \sum_{i=1}^N \sum_{k=1}^K \sum_{j=1}^K v_{kj}(\mathbf{x}_i + \mathbf{m}_{kj}) p(\mathbf{x}_1, \dots, \mathbf{x}_i + \mathbf{m}_{kj}, \dots, \mathbf{x}_N, t) \\ & - v_{kj}(\mathbf{x}_i) p(\mathbf{x}, t). \end{aligned} \quad (2.7)$$

The corresponding transition vector \mathbf{m}_{kj} is zero except for two components: $m_{kj,k} = 1$ and $m_{kj,j} = -1$.

By combining (2.2) and (2.7), we arrive at the RDME for a chemical system with reactions and diffusion

$$\frac{\partial p(\mathbf{x}, t)}{\partial t} = \mathcal{M}p(\mathbf{x}, t) + \mathcal{D}p(\mathbf{x}, t). \quad (2.8)$$

We now give a few comments on the validity of the RDME. Denote the molecular reaction radius by ρ_R and the shortest average life time of the molecular species by τ_{\min} [2]. Then the requirement for the size h of a cell is

$$\rho_R^2 \ll h^2 \ll \alpha \gamma \tau_{\min}, \quad (2.9)$$

where α is $\mathcal{O}(1)$ and depends on the cell shape and the dimension [10, 27]. Firstly, the upper bound guarantees that the mixing in a cell by diffusion is sufficiently fast for the molecules to be homogeneously distributed there. Another interpretation is that with slow diffusion, a better spatial resolution is necessary since the solution becomes less smooth. Secondly, there is also a *lower* bound on h for the modeling at a meso level to be meaningful. This lower bound guarantees that association and disassociation events can be properly localized within a computational cell. The model breaks down if we let $h \rightarrow 0$ despite the fact that there is often a meaningful stochastic partial differential equation (SPDE) in the limit. This SPDE, however, only remains valid as the first term in a system size expansion [16, Ch. 8.2]. It is understood with such an expansion that we are working on a scale where the cell size appears small but is still large enough to contain many molecules.

Let \mathcal{C}_k be a cell with a part of its boundary on $\partial\Omega$. Since there is no transport of molecules out from Ω at \mathcal{C}_k with the reactions in (2.4), the corresponding boundary condition at the macro level is a Neumann condition. Most results for the numerical solution of diffusive systems are derived under Dirichlet boundary conditions and we therefore now discuss the associated conditions for the RDME. Suppose that Ω is surrounded by a reservoir such that the number of molecules is fixed at the boundary $\partial\Omega$. Then $\mathbf{x}_{\cdot k}$ in those cells is given by the reservoir data. If $x_{ij} = 0$, then $v_{jk} = 0$ in (2.4) and there is no diffusion of molecules from the boundary to the interior cells, (cf. (2.4))

$$X_{ik} \rightarrow X_{ij} = \emptyset, v_{kj}(\mathbf{x}_{\cdot i}) = q_{kj}x_{ik}. \quad (2.10)$$

The transition vector \mathbf{m}_{kj} is zero except for $m_{kj,k} = 1$.

2.3 Relation to macroscopic equations

Define the concentrations ϕ_{ij} of species i in cell \mathcal{C}_j at a macroscopic level as the expected values of $|\mathcal{C}_j|^{-1}x_{ij}$. The RRE for ϕ_{ij} is obtained from the CME (2.2) by deriving equations for the mean values of x_{ij} as in [16, 27]. The system of ODEs defining the RRE is

$$\frac{d\phi_{ij}}{dt} = \omega_i(\phi_{\cdot j}) \equiv - \sum_{r=1}^R \frac{n_{ri}}{|\mathcal{C}_j|} w_r(|\mathcal{C}_j|\phi_{\cdot j}). \quad (2.11)$$

If there are no reactions but only diffusion, then a similar set of macroscopic equations may be derived. From the similarity between (2.2) and (2.7) we have

$$\begin{aligned} \frac{d\phi_{ij}}{dt} &= - \sum_{k=1}^K \frac{m_{kj,j}}{|\mathcal{C}_j|} v_{kj}(|\mathcal{C}_k|\phi_{\cdot i}) + \frac{m_{jk,j}}{|\mathcal{C}_j|} v_{jk}(|\mathcal{C}_j|\phi_{\cdot i}) \\ &= \sum_{k=1}^K \frac{|\mathcal{C}_k|}{|\mathcal{C}_j|} q_{kj} \phi_{ik} - \left(\sum_{k=1}^K q_{jk} \right) \phi_{ij}. \end{aligned} \quad (2.12)$$

The diffusion equation (2.12) has the form

$$\frac{d\phi_i^T}{dt} = \gamma D \phi_i^T \quad (2.13)$$

for each i (cf. (2.5)). The diffusion matrix has the elements $\gamma D_{jk} = q_{kj} |\mathcal{C}_k| / |\mathcal{C}_j|$, $j \neq k$, and $\gamma D_{jj} = -\sum_{k \neq j} q_{jk}$.

The positive coefficients q_{kj} in our diffusion model are non-zero only if cell k and j share a common point in 1D, a common edge in 2D, or a common facet in 3D. The diffusion matrix D therefore has a sparsity pattern matching the connectivity of the partitioning of Ω into computational cells.

Assume for now that the diffusion is isotropic on a Cartesian lattice in 1D with constant cell size h so that the probability q_{kj} to move from cell \mathcal{C}_k to cell \mathcal{C}_j is equal to the probability q_{jk} to move in the opposite direction. With isotropy, D has a particularly simple structure and is symmetric. For example, if $\Omega = [0, 1]$ with $h = 1/K$ and diffusion q we have that

$$\begin{aligned} \dot{\phi}_{i1} &= q(-\phi_{i1} + \phi_{i2}), \\ \dot{\phi}_{ij} &= q(\phi_{i,j-1} - 2\phi_{ij} + \phi_{i,j+1}), \quad j = 2, \dots, K-1, \\ \dot{\phi}_{iK} &= q(\phi_{i,K-1} - \phi_{iK}). \end{aligned} \quad (2.14)$$

Let $q = \gamma/h^2$ as in (2.5) and let $h \rightarrow 0$. Then the solution of (2.14) converges to the solution $\phi_i(x, t)$ of the diffusion equation in 1D

$$\frac{\partial \phi_i}{\partial t} = \gamma \frac{\partial^2 \phi_i}{\partial x^2}, \quad \frac{\partial \phi_i}{\partial x}(0, t) = \frac{\partial \phi_i}{\partial x}(1, t) = 0. \quad (2.15)$$

If boundary values ϕ_{i1} and ϕ_{iK} are given, then the solution converges to the solution of the PDE in (2.15) with boundary conditions $\phi_i(0, t) = \phi_{i1} = g_{i0}$ and $\phi_i(1, t) = \phi_{iK} = g_{i1}$ for some $g_{i0}, g_{i1} \geq 0$.

Suppose that the interior of $\Omega = [0, 1] \times [0, 1]$ is covered by square cells of size $h \times h$ in 2D or that $\Omega = [0, 1] \times [0, 1] \times [0, 1]$ in 3D and partitioned into cubic cells of size $h \times h \times h$. In both cases, D is symmetric and will approximate the Laplacian Δ with Neumann boundary conditions. With the normal derivative of ϕ_i at the boundary $\partial\Omega$ written as $\partial\phi_i/\partial n$, the solution ϕ_i converges when $h \rightarrow 0$ to the solution of

$$\frac{\partial \phi_i}{\partial t} = \gamma \Delta \phi_i \text{ in } \Omega, \quad \frac{\partial \phi_i}{\partial n} = 0 \text{ on } \partial\Omega, \quad (2.16)$$

If ϕ_i is given data in the boundary cells, then the boundary conditions in (2.16) will be Dirichlet type, $\phi_i = g_i$ on $\partial\Omega$.

The macroscopic approximation of the diffusive part of (2.8) with a vanishing cell size in a Cartesian mesh thus satisfies a diffusion equation (2.15). The macroscopic counterpart to \mathcal{M} in (2.8) is the RRE (2.11). A macroscopic concentration ϕ_i affected by both chemical reactions and diffusion fulfills a RDE

$$\frac{\partial \phi_i}{\partial t} = \omega_i(\phi) + \gamma \Delta \phi_i, \quad i = 1, \dots, N. \quad (2.17)$$

A Cartesian mesh for discretization of $\Delta\phi$ has many advantages but is impractical for curved inner and outer boundaries of Ω . A RDME on unstructured meshes is proposed in Section 3.

2.4 Relation to microscopic equations

If we consider pure diffusion in 1D, it is possible to directly compare the coefficients obtained from the finite element discretization with the expected value of the first exit time of Brownian motion from a finite interval. Using linear basis functions in a FEM discretization of (2.15) on a mesh with vertices x_j and cell sizes $h_j = x_j - x_{j-1}$, in the interior of Ω the non-zero entries of the stiffness matrix S and the mass matrix M are

$$\begin{aligned} \gamma S_{j,j-1} &= \frac{\gamma}{h_j}, & \gamma S_{j,j+1} &= \frac{\gamma}{h_{j+1}}, & \gamma S_{jj} &= -\frac{\gamma}{h_j} - \frac{\gamma}{h_{j+1}}, \\ M_{j,j-1} &= \frac{1}{6}h_j, & M_{j,j+1} &= \frac{1}{6}h_{j+1}, & M_{jj} &= \frac{1}{3}(h_j + h_{j+1}). \end{aligned} \quad (2.18)$$

After mass lumping the coefficients corresponding to jumps from node j to its neighbors in (2.5) are given by

$$q_{j,j-1} = \frac{2\gamma}{h_j(h_j + h_{j+1})}, \quad q_{j,j+1} = \frac{2\gamma}{h_{j+1}(h_j + h_{j+1})}. \quad (2.19)$$

Consequently, the exponentially distributed waiting time for the next event at node j has the expected value

$$q_{j,j-1} + q_{j,j+1} = \frac{2\gamma}{h_j h_{j+1}}. \quad (2.20)$$

On a uniform grid we recover the jump coefficients γ/h^2 and the parameter $2\gamma/h^2$ used in [23].

Interpreted as the average time for a Brownian particle starting at node x_j to reach either of its neighbors, we can compare the value in (2.20) with the actual expected value of the first exit time $\tau = \inf\{t : \xi_t \notin (x_{j-1}, x_{j+1})\}$ where ξ_t is defined in (2.6). A straightforward application of Dynkin's formula [48, Ch. 7.4] yields

$$E_{x_j}[\tau]^{-1} = \frac{2\gamma}{h_j h_{j+1}}, \quad (2.21)$$

in accordance to (2.20). The probabilities to exit at x_{j-1} and x_{j+1} respectively are given by $h_{j+1}/(h_j + h_{j+1})$ and $h_j/(h_j + h_{j+1})$, and using this we recover the jump coefficients (2.19). In this sense, the coefficients of the mesoscale model obtained from the discretization of the macroscale equation is consistent with the microscale description. It is worth noticing however, that τ is not generally exponentially distributed [4, p. 212].

3 Diffusion coefficients

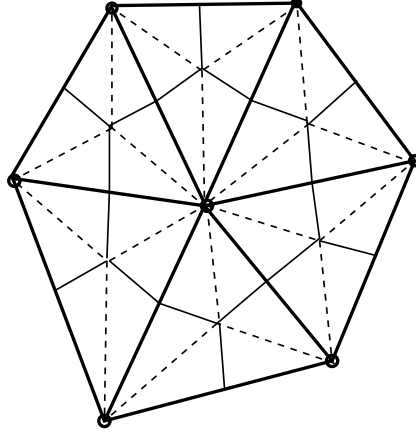


Figure 3.1: The primal mesh (thick lines) with the vertices (small circles), the dual mesh (thin lines) and the bisectors of the triangles (dashed lines).

Consider a part of an unstructured mesh in 2D covering Ω with a polygonal boundary $\partial\Omega$ in Figure 3.1. The primal mesh consists of triangles with the vertices in the corners. The cells \mathcal{C}_k in the dual mesh are polygons and in the interior of Ω , the center of \mathcal{C}_k is the vertex k . The edges of the polygon coincide with a part of the bisectors of the triangles or with the boundary $\partial\Omega$. The corners of an inner \mathcal{C}_k are the barycenters of the triangles and the midpoints of the edges from its center vertex. In 1D, the cell in the primal mesh is a line segment with a vertex in both ends and the dual mesh also consists of line segments shifted with respect to the primal mesh and a vertex in the center. The primal cell is a tetrahedron and the dual cell is a polyhedron in 3D.

Similarly, the dual cells \mathcal{C}_k in a Cartesian structured mesh in 2D with vertices $(ih, jh), i = 0, \dots, K, j = 0, \dots, K$, are the cells in the staggered mesh. In the interior of Ω , the vertices are in the center of \mathcal{C}_k .

A finite element discretization of the RDE in (2.17) with continuous, piecewise linear basis and test functions on the primal unstructured mesh generates a system of equations to solve for the nodal values ϕ . The components of ϕ are $\phi_{ij}(t)$, the concentration of species i in vertex j at time t [44, Ch. 15] but can also be interpreted as the mean value of the concentration of species i in the dual cell \mathcal{C}_j . The system of equations is [44, Ch. 14]

$$\hat{M}\dot{\phi} = \mathbf{f}(\phi) + \gamma\hat{S}\phi. \quad (3.1)$$

The mass matrix \hat{M} and the stiffness matrix \hat{S} are symmetric, \hat{M} is positive definite and \hat{S} is negative semi-definite with Neumann boundary conditions and negative definite with Dirichlet conditions. The reaction terms are represented

by the nonlinear term \mathbf{f} . If h is a suitable measure of the sizes of the triangles in the mesh, then the error in the FEM solution of the Dirichlet problem in the L_2 -norm is $\mathcal{O}(h^2)$ [44, Ch. 14].

Order the unknowns in ϕ according to a linear index so that

$$\phi = (\phi_1, \dots, \phi_i, \dots, \phi_N)^T. \quad (3.2)$$

Then \hat{M} and \hat{S} are block diagonal matrices where the blocks M and S are identical, small mass and stiffness matrices. The system (3.1) is simplified by introducing mass lumping of M and \mathbf{f} . Let \hat{A} be a diagonal matrix with diagonal blocks A with $A_{jj} = \sum_{k=1}^K M_{jk}$ and let similarly $\bar{\mathbf{f}}$ be the lumped version of \mathbf{f} . In 1D, A_{jj} is the length of the dual cell with vertex j in the center, see (2.18). Similarly in 2D, A_{jj} is the area $|\mathcal{C}_j|$ of the dual cell in Figure 3.1 with vertex j in the center [44, Ch. 15] and in 3D, A_{jj} is the volume of \mathcal{C}_j [45]. The simplified system (3.1) is now

$$\dot{\phi} = \hat{\omega}(\phi) + \gamma \hat{D}\phi, \quad \hat{\omega} \equiv \hat{A}^{-1}\bar{\mathbf{f}}, \quad \hat{D} \equiv \hat{A}^{-1}\hat{S}, \quad (3.3)$$

which is our approximation of (2.17). The solution ϕ of (3.3) is also generally second order accurate in 2D [35].

Let D denote a block on the diagonal of \hat{D} . Then $D = A^{-1}S$ and an off-diagonal component D_{jk} is non-zero only if two vertices j and k are connected by an edge. With Neumann conditions, the diagonal blocks D satisfy $D_{jj} = -\sum_{k \neq j} D_{jk}$ so that $\sum_{k=1}^K D_{jk} = 0$ for every j . In other words, the constant vector $\mathbf{e}_1 = (1, 1, \dots, 1)^T$ is in the null-space of D and is the right eigenvector with eigenvalue zero. The corresponding left eigenvector \mathbf{e}_2 has the diagonal elements of A as components, $e_{2j} = A_{jj}$. Let

$$\bar{x}_{ij} = \sum_{\mathbf{x}} x_{ij} p(\mathbf{x}, t) = |\mathcal{C}_j| \phi_{ij}$$

denote the expected value of the number of molecules of species i in cell j . In a system without reactions, by (3.3)

$$0 = \gamma \mathbf{e}_2^T \hat{D} \phi_i^T = \frac{d}{dt} \mathbf{e}_2^T \phi_i^T = \frac{d}{dt} \sum_{j=1}^K A_{jj} \phi_{ij} = \frac{d}{dt} \sum_{j=1}^K |\mathcal{C}_j| \phi_{ij} = \frac{d}{dt} \sum_{j=1}^K \bar{x}_{ij}, \quad (3.4)$$

i.e. the total number of molecules of each species are conserved by the diffusion. This is not the case with Dirichlet conditions, where $D_{jj} \leq -\sum_{k \neq j} D_{jk}$ and D is non-singular.

By the calculation in Section 2.4 in 1D, we find that $D_{jk} > 0$ if $k = j - 1$ or $k = j + 1$ and zero for the other non-diagonal entries. If the mesh in 2D is a Delaunay triangulation [17], then the Voronoi cells are close to the cells in the dual mesh defined by Figure 3.1. Two triangles share an edge in Figure 3.2a. The

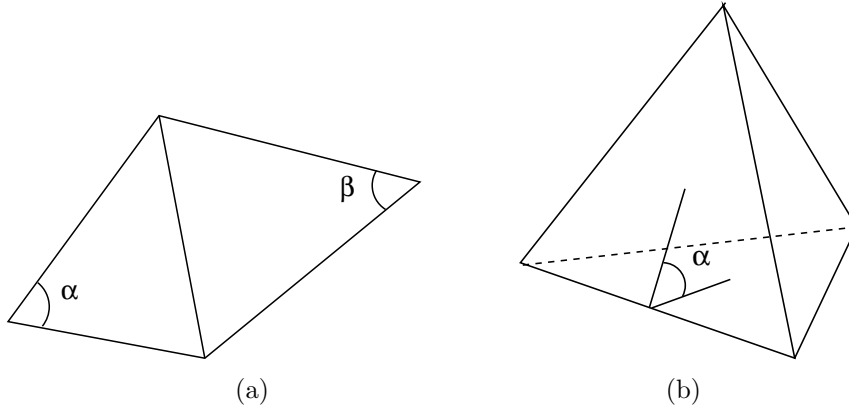


Figure 3.2: The critical angles in 2D (a) and 3D (b) for positive off-diagonal elements in the stiffness matrix.

sum of the two opposing angles α and β in the triangles is less than or equal to π in a Delaunay triangulation and $D_{jk} \geq 0$ when $j \neq k$ [46]. In 3D, assume that the dihedral angle at an edge between two facets of a tetrahedron, see Figure 3.2b, is non-obtuse ($\alpha \leq \pi/2$) for all tetrahedra in the mesh. Then the elements of D all have the right sign [46]. With these properties of the discretization and without chemical reactions, a discrete maximum principle is fulfilled [46] for Dirichlet boundary conditions ensuring that with non-negative initial conditions the solution remains non-negative. The diffusion matrix D generated by the FEM discretization of Δ in (2.17) has the same properties as the diffusion matrix in (2.13). A review of these triangulations in three and higher dimensions is found in [5]. They may not be trivial to generate in higher dimensions than 2.

Discretization matrices of second order PDEs are frequently *M-matrices* [20, 10.3]. Henceforth, we shall assume the following slightly weaker property:

Assumption 3.1 *The diffusion matrix D for Dirichlet and Neumann boundary conditions fulfills for $j \neq k$,*

$$D_{jk} \geq 0, \quad D_{jj} < 0, \quad \sum_{k=1}^K D_{jk} \leq 0.$$

The last inequality is an equality for Neumann conditions.

The macroscopic elements in γD in (3.3) define the coefficients q_{kj} in the mesoscopic model of diffusion (2.4). The diffusion matrix D in (2.13) has the form $\gamma D = A^{-1}QA$, where $Q_{jk} = q_{kj}$ when $j \neq k$. Since D in (2.13) and (3.3) are identical we have

$$Q = \gamma SA^{-1} = \gamma D^T. \tag{3.5}$$

Except for the case when all cells have the same size, Q is generally unsymmetric.

The concentrations ϕ_{ij} defined as the expected values of x_{ij}/A_{jj} with the PDF in (2.8) will satisfy (3.3). The molecules at the meso level can jump between dual cells with a point (1D), edge (2D), or facet (3D) in common since $D_{jk} > 0$ there. The connectivity graph of D tells in which direction a molecule can diffuse and the positive elements of D are inversely proportional to the expected value of the first exit time to leave the cell, cf. (2.5) and Section 2.4.

An alternative to the finite element discretization of the RDE in (2.17) is to use the finite volume method (FVM). Here, the averages of the concentrations $\bar{\phi}_{ij}$ in the dual cells are the degrees of freedom. Then

$$\begin{aligned} \frac{\partial \bar{\phi}_{ij}}{\partial t} &= \frac{1}{|\mathcal{C}_j|} \int_{\mathcal{C}_j} \frac{\partial \phi_i}{\partial t} dV = \frac{1}{|\mathcal{C}_j|} \int_{\mathcal{C}_j} \omega_i(\phi) + \gamma \nabla \cdot \nabla \phi_i dV \\ &= \frac{1}{|\mathcal{C}_j|} \int_{\mathcal{C}_j} \omega_i(\phi) dV + \frac{1}{|\mathcal{C}_j|} \int_{\partial \mathcal{C}_j} \gamma \hat{\mathbf{n}} \cdot \nabla \phi_i dS, \end{aligned} \quad (3.6)$$

where Gauss' theorem has been used and $\hat{\mathbf{n}}$ is the normal of $\partial \mathcal{C}_j$. The reaction term in \mathcal{C}_j is approximated by $\omega_i(\phi_j)$. The gradient $\nabla \phi_i$ is needed on the boundary of \mathcal{C}_j and different approximations are possible. A simple one is to let $\hat{\mathbf{n}} \cdot \nabla \phi_i \approx (\phi_{ik} - \phi_{ij})/h_{jk}$ where h_{jk} is the distance between vertex j and a neighboring vertex k . The resulting diffusion term is in \mathcal{C}_j ,

$$\sum_k c_{jk} (\phi_{ik} - \phi_{ij}) / h_{jk},$$

with summation over those vertices with an edge between j and k and where c_{jk} equals the size of the edges or facets of $\partial \mathcal{C}_j$ adjacent to the same edge. Then the coefficients in this discretization are interpreted as the diffusion coefficients in (2.7) in the same manner as in the FEM case. The difference between (3.6) and (3.3) lies in the approximation of the diffusion term.

Convergence of the FVM to the analytical solution is proved for certain discretizations of the gradient in [13, 25] but the quality of the approximation seems to depend critically on the quality of the mesh [43]. This is one of the reasons why we prefer the FEM approach. Another reason is that FVM is perhaps more suitable for problems dominated by convection while chemical systems from molecular biology tend to be of diffusive character.

4 Moments of the diffusion

The purpose of this section is to prove that the diffusion can be accurately evolved deterministically when the number of diffusing molecules is sufficiently large. Consider the equations for the moments of \mathbf{x} in a system with diffusion and Neumann boundary conditions but without chemical reactions. The expected

values and the covariance matrices satisfy systems of ODEs. These equations are derived in [12, 27] for general propensities, but with

$$v_{kj}(\mathbf{x}_i) = Q_{jk}x_{ik}, \quad j \neq k,$$

being linear (cf. (2.4)), they have a particularly simple structure.

Applying the formulas in [12, 15] or invoking (2.13), the first moment of the number of molecules of species i in a cell is given by

$$\dot{\bar{\mathbf{x}}}_i^T = Q\bar{\mathbf{x}}_i^T. \quad (4.1)$$

This equation is exact since the diffusion propensities v_{kj} are linear in \mathbf{x} and no coupling to higher order moments exists.

The second moments or covariances of any species i between cells j and k are denoted by C_{jk} . The equation for C_{jk} is

$$\dot{C}_{jk} = \sum_{l=1}^K Q_{kl}C_{jl} + \sum_{l=1}^K Q_{jl}C_{kl} + F_{jk}, \quad j, k = 1, \dots, K, \quad (4.2)$$

with the driving term F defined by

$$F_{jk} = \sum_{\alpha=1}^K \sum_{\beta=1}^K m_{\alpha\beta,j} m_{\alpha\beta,k} v_{\alpha\beta}(\bar{\mathbf{x}}_i).$$

This can be written in matrix form since C is symmetric,

$$\dot{C} = CQ^T + QC + F. \quad (4.3)$$

Using the properties of the diffusion propensities, the elements of F are

$$F_{jj} = \sum_{l=1, l \neq j}^K Q_{jl}\bar{x}_{il} + Q_{lj}\bar{x}_{ij}, \quad F_{jk} = -(Q_{jk}\bar{x}_{ik} + Q_{kj}\bar{x}_{ij}), \quad j \neq k, \quad (4.4)$$

The covariance equation is also exact for the same reason as before.

The solution of (4.1) can be written

$$\bar{\mathbf{x}}_i(t) = \bar{\mathbf{x}}_i^0 \exp(Q^T t), \quad (4.5)$$

where $\bar{\mathbf{x}}_i^0$ is the initial value at $t = 0$. The eigenvalues of Q and D are all negative except for one which is zero. The corresponding left eigenvector of Q is \mathbf{e}_1 and the right eigenvector is \mathbf{e}_2 , both of them defined in Section 3. Hence,

$$\bar{\mathbf{x}}_i(t) = \kappa_i \mathbf{e}_2^T + \delta \bar{\mathbf{x}}_i(t). \quad (4.6)$$

with an upper bound on $\|\delta\bar{\mathbf{x}}_i(t)\|$ given by $c_\delta \exp(\lambda_2 t)$ where λ_2 is the negative eigenvalue of Q with smallest magnitude and the norm is the ℓ_2 -norm. Therefore,

$$\lim_{t \rightarrow \infty} \bar{\mathbf{x}}_i(t) = \kappa_i \mathbf{e}_2^T. \quad (4.7)$$

By (3.4), $\bar{\mathbf{x}}_i \cdot \mathbf{e}_1$ is constant and we obtain

$$\kappa_i \mathbf{e}_2^T \mathbf{e}_1 = \bar{\mathbf{x}}_i^0 \cdot \mathbf{e}_1 \Rightarrow \kappa_i = \sum_{j=1}^K \bar{\mathbf{x}}_{ij}^0 / \sum_{j=1}^K A_{jj}. \quad (4.8)$$

The explicit solution of (4.3) is

$$C(t) = \exp(Qt)C_0 \exp(Q^T t) + \int_0^t \exp(Q(t-s))F \exp(Q^T(t-s)) ds, \quad (4.9)$$

where C_0 is the initial value of the covariance at $t = 0$. Using (4.4), (4.6), (4.7), and (3.5) we find that when $t \rightarrow \infty$

$$\begin{aligned} F_{jj} &= \gamma \kappa_i \sum_{l=1, l \neq j}^K A_{ll} S_{jl} / A_{ll} + A_{jj} S_{lj} / A_{jj} = 2\gamma \kappa_i \sum_{l=1, l \neq j}^K S_{jl} = -2\gamma \kappa_i S_{jj}, \\ F_{jk} &= -\gamma \kappa_i (A_{kk} S_{jk} / A_{kk} + A_{jj} S_{kj} / A_{jj}) = -2\gamma \kappa_i S_{jk}, \quad j \neq k, \end{aligned}$$

and hence that,

$$F = -2\gamma \kappa_i S + \delta F, \quad (4.10)$$

where $\|\delta F\|$ is bounded by $c_{\delta F} \exp(\lambda_2 t)$. A bound on the covariance matrix for finite time is derived in the next proposition.

Proposition 4.1 *Suppose that $C_0 = 0$. Then*

$$\|C(t)\| \leq c_F \frac{\max_j A_{jj}}{\min_j A_{jj}} \int_0^t \|\bar{\mathbf{x}}_i\| ds, \quad (4.11)$$

for some bounding constant c_F such that $\|F\| \leq c_F \|\bar{\mathbf{x}}_i\|$.

Proof. Let $\tilde{S} = A^{-1/2} S A^{-1/2}$. Then

$$\exp(Qt) = \exp(\gamma S A^{-1} t) = A^{1/2} \exp(\gamma \tilde{S} t) A^{-1/2}.$$

The symmetric matrix $\gamma \tilde{S}$ has the same eigenvalues as Q . Let the unitary matrix U have the eigenvectors of \tilde{S} as columns and let Λ have the corresponding eigenvalues on the diagonal. A bound on the exponential of $Q\tau$ with $\tau \geq 0$ is

$$\begin{aligned} \|\exp(Q\tau)\| &\leq \|A^{1/2}\| \|A^{-1/2}\| \|U \exp(\gamma \Lambda \tau) U^T\| \\ &\leq \|\exp(\gamma \Lambda \tau)\| \max_j \sqrt{A_{jj}} / \min_j \sqrt{A_{jj}} \leq \max_j \sqrt{A_{jj}} / \min_j \sqrt{A_{jj}}. \end{aligned}$$

The same bound is valid for $\exp(Q^T \tau)$. Hence,

$$\begin{aligned} & \left\| \int_0^t \exp(Q(t-s)) F \exp(Q^T(t-s)) ds \right\| \\ & \leq \int_0^t \|F\| \max_j A_{jj} / \min_j A_{jj} ds \leq c_F \frac{\max_j A_{jj}}{\min_j A_{jj}} \int_0^t \|\mathbf{x}_i\| ds. \end{aligned}$$

□

Remark. Using (4.9) and (4.10), one can show that $\|C(t)\|$ is bounded when $t \rightarrow \infty$. If $C_0 = 0$, then $\|C(t)\| \sim \kappa_i$ for large t . □

It follows from the proposition that the variance of \mathbf{x}_i is proportional to $\|\bar{\mathbf{x}}_i\|$ in a bounded time interval so that the standard deviation is proportional to $\sqrt{\|\bar{\mathbf{x}}_i\|}$. When t is large then $\bar{\mathbf{x}}_i$ in (4.7) is of the same order as κ_i , a weighted average of the initial $\bar{\mathbf{x}}_i^0$ (4.8). The standard deviation is proportional to $\sqrt{\kappa_i}$ according to the remark after Proposition 4.1. Therefore, the quotient between the standard deviation and the expected value is small for large copy numbers implying that the expected value is indeed a good approximation. Conversely, if the number of molecules in a cell is small, then a description in terms of expectation values should not be used.

5 Time integration and hybrid diffusion

For a discretization parameterized by the cell size h , the time to compute a trajectory of a system with SSA spent in the diffusion part of (2.8) is proportional to $x\gamma/h^2$, where x is the total number of diffusing molecules (cf. (2.4) and (2.5)). It follows that diffusion is the only event with a *total* intensity that increases with increasing spatial resolution. In order to avoid this, we propose to split the diffusion operator \mathcal{D} into two parts with the species with low copy numbers in \mathcal{D}_L and the species with high copy numbers in \mathcal{D}_H . The diffusion in \mathcal{D}_H can then be advanced in time macroscopically.

Order the species X_i such that X_i , $i = 1, \dots, N_L$, have low copy numbers and X_i , $i = N_L + 1, \dots, N$, have high numbers and let

$$\begin{aligned} \xi_i & \equiv \sum_{k=1}^K \sum_{j=1}^K v_{kj}(\mathbf{x}_i + \mathbf{m}_{kj}) p(\mathbf{x}_1, \dots, \mathbf{x}_i + \mathbf{m}_{kj}, \dots, \mathbf{x}_N, t) - v_{kj}(\mathbf{x}_i) p(\mathbf{x}, t), \\ \mathcal{D}_L p(\mathbf{x}, t) & \equiv \sum_{i=1}^{N_L} \xi_i, \quad \mathcal{D}_H \equiv \mathcal{D} - \mathcal{D}_L. \end{aligned} \tag{5.1}$$

The operator on the right hand side of (2.8) can be written

$$\frac{\partial p(\mathbf{x}, t)}{\partial t} = [\mathcal{M} + \mathcal{D}_L] p(\mathbf{x}, t) + \mathcal{D}_H p(\mathbf{x}, t). \tag{5.2}$$

It follows from Section 4 that the effect of diffusion on the species with many molecules in each cell is well approximated by the mean-field equations. In the numerical solution procedure, the second part of (5.2) is therefore first advanced half a time step $\Delta t/2$ with the macroscopic diffusion. Then the first part is integrated a full step Δt and finally the macroscopic diffusion is applied for half a time step again. This is the Strang splitting procedure [41] to solve (5.2) and below we give conservative conditions under which both steps preserve the non-negativity of the solution.

For many relevant cases, a single trajectory gives sufficient insight into the stochastic reaction-diffusion system but the same procedure also works well for simultaneous simulation of M trajectories. An application could be to approximate the PDF by following an ensemble of trajectories with state vectors $\mathbf{x}^m(t)$, $m = 1, \dots, M$. Then p is reconstructed according to

$$p(\mathbf{x}, t^n) \approx \frac{1}{M} \sum_{m=1}^M \Psi^m, \quad \Psi^m = \begin{cases} 1, & \mathbf{x}^m(t^n) = \mathbf{x}, \\ 0, & \text{otherwise.} \end{cases} \quad (5.3)$$

In order to advance the trajectories Δt in time from t^n to t^{n+1} , each trajectory is first integrated in time from t^n to $t^n + \Delta t/2$ by solving (4.1) for the species $i = N_L + 1, \dots, N$. The time derivative in (4.1) is discretized by the trapezoidal (or Crank-Nicolson) method of second order temporal accuracy and the new state $\mathbf{x}_i^{n+1/4}$ for each trajectory is the solution of

$$(I - \frac{1}{2}\Delta t Q)(\mathbf{x}_i^{n+1/4})^T = (I + \frac{1}{2}\Delta t Q)(\mathbf{x}_i(t^n))^T, \quad i = N_L + 1, \dots, N. \quad (5.4)$$

Alternatively, a scheme with an error $\mathcal{O}(\Delta t)$ is the Euler backward method

$$(I - \frac{1}{2}\Delta t Q)(\mathbf{x}_i^{n+1/4})^T = (\mathbf{x}_i(t^n))^T. \quad (5.5)$$

The time step in the Strang splitting must be sufficiently small to resolve the shortest time scale of the reactions τ_{\min} in (2.9). Thus, we can take $\Delta t \sim \tau_{\min}$ and by (2.9) and [10]

$$h^2 \ll \alpha \gamma \Delta t. \quad (5.6)$$

For such a time step, an explicit method for integration of (4.1) would be very inefficient. Only an implicit method suitable for stiff problems, such as the trapezoidal method, can efficiently advance the solution of (4.1) in time in a stable manner.

The next step is to evolve the M trajectories with SSA [19] for one time step Δt using the reduced master equation

$$\frac{\partial p(\mathbf{x}, t)}{\partial t} = \mathcal{M}p(\mathbf{x}, t) + \mathcal{D}_L p(\mathbf{x}, t). \quad (5.7)$$

If Δt is short then there may be no events in many of the realizations of the process and some computational work will be wasted.

The final step is to evolve each trajectory \mathbf{x}_i^m half a time step again using the macroscopic diffusion. The result is an approximative sample of p in (5.2) at time t^{n+1} .

The error due to the Strang splitting and the time discretization by the trapezoidal method is $\mathcal{O}(\Delta t^2)$. Similarly, the error due to the FEM approximation of the diffusion is $\mathcal{O}(h^2)$ [44, Ch. 7].

It is more difficult to estimate the error induced from using the macroscopic diffusion without being overly pessimistic. A bound on the local *single trajectory* error can be obtained as follows. Write $\|C(\Delta t)\| = \mathcal{O}(\Delta t \|\bar{\mathbf{x}}_i\|)$ by Proposition 4.1. Then the local stochastic error (standard deviation) relative to $\bar{\mathbf{x}}_i$ is $\mathcal{O}(\Delta t^{1/2} \|\bar{\mathbf{x}}_i\|^{-1/2})$ for $i > N_L$ since only species with high copy numbers participate in the macroscopic diffusion. This simple bound, however, gives no global estimate since reasonable and sufficient stability properties of the system are difficult to prescribe. When using deterministic diffusion for some species it must simply be regarded as given *a priori* that the diffusion noise for those variables has little or no impact on the system as a whole. Note that computing averages in order to approximate expected values will generally make this error substantially smaller since the macroscopic diffusion is *exact* in expectation (cf. (4.1)).

In a system with only diffusion, the algorithm has the following two properties.

Proposition 5.1 *Assume that D satisfies Assumption 3.1, that $\mathbf{x}^m(0) \geq 0$ for all trajectories $m = 1, \dots, M$, and that $\Delta t \leq h_{\min}^2/6\gamma$ for the trapezoidal method in (5.4), where h_{\min} is the minimal distance between a vertex and the opposing edge in a triangle in the mesh. Then in a system without chemical reactions, the copy numbers in the trajectories computed by the hybrid algorithm remain non-negative for $t > 0$. For the Euler backward method (5.5), there is no time step restriction for non-negativity.*

Proof. If D satisfies Assumption 3.1, then Q satisfies the assumption by (3.5). Let $(\mathbf{x}_i(t^n))^T = A^{1/2} \mathbf{y}^n$ in a symmetrization of (5.4). Then

$$(I - \tilde{S}) \mathbf{y}^{n+1/4} = (I + \tilde{S}) \mathbf{y}^n = \mathbf{g}, \quad \tilde{S} = 0.5\gamma \Delta t A^{-1/2} S A^{-1/2}.$$

The symmetric matrix \tilde{S} has components $\tilde{S}_{jk} \geq 0$, $j \neq k$, and $\tilde{S}_{jj} < 0$ and $I - \tilde{S}$ is positive definite since \tilde{S} is negative semi-definite. By [44, Lemma 15.4], $(I - \tilde{S})_{jk}^{-1} \geq 0$ and by [44, Theorem 15.6] if $\Delta t \leq h_{\min}^2/6\gamma$ and $\mathbf{y}^n \geq 0$, then the right hand side \mathbf{g} is non-negative. Consequently,

$$\mathbf{y}^{n+1/4} = (I - \tilde{S})^{-1} \mathbf{g} \geq 0,$$

and therefore $\bar{\mathbf{x}}_i^{n+1/4} \geq 0$. The only differences for the Euler backward method are that the right hand side \mathbf{g} equals \mathbf{y}^n and is always non-negative and \tilde{S} is

twice as large. The intermediate SSA-step also preserves the non-negativity as do the final step. Thus, the copy numbers of the species computed by the hybrid algorithm remain non-negative. \square

Remark. The upper bound on Δt in the proposition is quite restrictive considering the requirements for resolving the reactive time scale in the splitting in (5.6). In practice the solutions in the macroscopic diffusion step stay non-negative with much longer Δt since the mean values are large for the species involved in \mathcal{D}_{Hp} . \square

Proposition 5.2 *In a system with only diffusion and $\sum_k D_{jk} = 0$, $j = 1, \dots, K$, the total number of molecules of each species in a trajectory is constant.*

Note that the exact solution to the equations for the concentrations has the same property in (3.4).

Proof. The vector \mathbf{e}_1 satisfies $D\mathbf{e}_1 = 0$ and $\mathbf{e}_1^T Q = \mathbf{e}_1^T D^T = 0$. In the first step of the hybrid algorithm (5.4), we have

$$\mathbf{e}_1^T (I - \frac{1}{2}\Delta t Q)(\mathbf{x}_i^{n+1/4})^T = \mathbf{e}_1^T (\mathbf{x}_i^{n+1/4})^T = \mathbf{e}_1^T (I + \frac{1}{2}\Delta t Q)(\mathbf{x}_i(t^n))^T = \mathbf{e}_1^T (\mathbf{x}_i(t^n))^T.$$

Consequently,

$$s_i^{n+1/4} \equiv \sum_{m=1}^M \sum_{j=1}^K x_{ij}^{m,n+1/4} = \sum_{m=1}^M \sum_{j=1}^K x_{ij}^{m,n} \equiv s_i^n, \quad i = N_L + 1, \dots, N,$$

and s_i , the sum of the copy number of species i over all cells, is thus preserved by (5.4). This sum over all cells is also preserved by diffusion simulated by SSA in every trajectory in the intermediate step in the hybrid algorithm. Finally, s_i is preserved in the last step of the Strang splitting. \square

The accuracy and efficiency of the algorithm are evaluated in the next section.

6 Numerical results

The algorithm for the RDME in Section 5 is applied to the diffusion equation and to two different systems from molecular biology. The convergence of samples from the mesoscopic diffusion model to the solution of the macroscopic equation is illustrated in Section 6.1. The method is applied to a model of a bi-stable reaction network in Section 6.2. Finally, in Section 6.3 we illustrate the potential of the hybrid method by comparing it to a purely stochastic simulation. The meshes, the stiffness and the mass matrices are generated using the PDE-toolbox [31] in MATLAB.

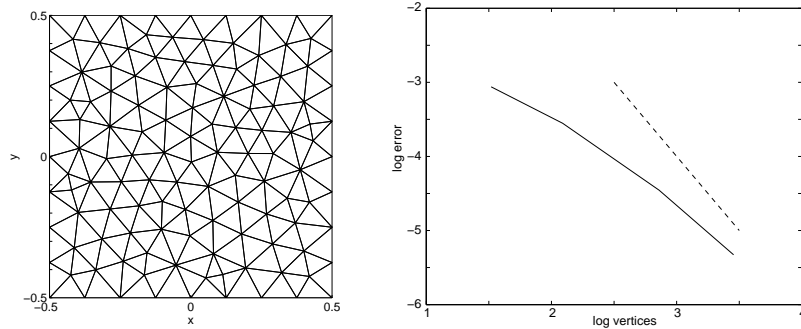


Figure 6.1: The triangular mesh with 123 vertices (left) and the logarithm of the error vs. the number of vertices (right). The ℓ_2 -norm of the error (solid) is compared to the asymptotic rate of convergence (dashed).

6.1 Diffusion

The diffusion equation with Neumann boundary conditions and initial data

$$\begin{aligned} u_t &= \gamma(u_{xx} + u_{yy}), \text{ in } \Omega = [-0.5, 0.5] \times [-0.5, 0.5], \quad \gamma = 10^{-3}, \\ \frac{\partial u}{\partial n} &= 0, \text{ on } \partial\Omega, \quad u(x, y, 0) = 100(1 - \cos(2\pi x)), \end{aligned}$$

has the analytical solution

$$u_a(x, y, t) = 100(1 - \cos(2\pi x) \exp(-4\gamma\pi^2 t)). \quad (6.1)$$

The solution u_d is computed with a FEM discretization of the space derivatives with mass lumping and integrated in time by the trapezoidal method as in (5.4). The error $u_d - u_a$ in the vertices in the ℓ_2 -norm is $\mathcal{O}(\Delta t^2) + \mathcal{O}(h^2)$, see Section 5. The behavior of the spatial error at $t = 1$ is confirmed in Figure 6.1. Asymptotically, when the number of vertices increases the theoretical rate is obtained.

A stochastic simulation of the diffusion with m molecules in the mesh is compared with the analytical and the FEM solutions in Table 6.1. Two meshes are used: one with 33 vertices and a maximum length h_{max} of an edge of a triangle equal to 0.5 and one with 123 vertices and $h_{max} = 0.25$ (see Figure 6.1). Each stochastic simulation starts with 100 molecules distributed according to $u(x, y, 0)$. The average concentrations u_m in the cells \mathcal{C}_k are computed for M trajectories such that $m = 100M$. Then u_m is compared to u_a and u_d in the vertices at $t = 1$. The weighted vector norms in ℓ_2 and ℓ_∞ are defined by

$$\|u\|_2^2 = \sum_j u_j^2 |\mathcal{C}_j|, \quad \|u\|_\infty = \max_j |u_j|. \quad (6.2)$$

The differences in these norms divided by the system size 100, $\delta_a = (u_m - u_a)/100$ and $\delta_d = (u_m - u_d)/100$, for two different discretizations are collected in Table 6.1.

$\log_{10} m$	ℓ_2				ℓ_∞			
	$h_{max} = 0.5$		$h_{max} = 0.25$		$h_{max} = 0.5$		$h_{max} = 0.25$	
	δ_a	δ_d	δ_a	δ_d	δ_a	δ_d	δ_a	δ_d
2	.038	.038	.1	.1	.52	.53	4.5	4.5
3	.019	.018	.029	.029	.32	.31	1.2	1.2
4	.0053	.0053	.0073	.0073	.091	.096	.23	.23
5	.0018	.0016	.0029	.0030	.031	.017	.16	.17
6	.0011	.00057	.0011	.0010	.016	.0093	.047	.042
7	.00083	.00015	.00039	.00027	.013	.0023	.014	.010

Table 6.1: The relative difference between the stochastic solution and the analytic solution δ_a or the FEM solution δ_d for different mesh sizes h_{max} and total number of molecules m .

The error is expected to behave as $\mathcal{O}(h_{max}^2) + \mathcal{O}(m^{-1/2})$ and this is what we observe in the table. The difference between u_m and u_d decays with increasing m at the correct rate in both norms. In the example in Figure 6.1, the ℓ_2 -error is $8.7 \cdot 10^{-4}$ when $h_{max} = 0.5$ and $2.8 \cdot 10^{-4}$ when $h_{max} = 0.25$ explaining the difference between δ_a and δ_d in Table 6.1. When m is large then the dominant term in δ_a is the discretization error.

6.2 Domain separation in a bi-stable system

In this section we simulate a model of a bi-stable system, previously investigated using the freely available software MesoRD [23] in [10]. The model consists of eight chemical species participating in twelve reactions, see Table 6.2. Being based on a double negative feedback mechanism, in the spatially homogeneous case the system switches between states with mostly A molecules and states where B is dominating. The model is used to illustrate and explain the observation that global bi-stability can be lost in a spatially dependent system due to domain separation, when the diffusion is slow.

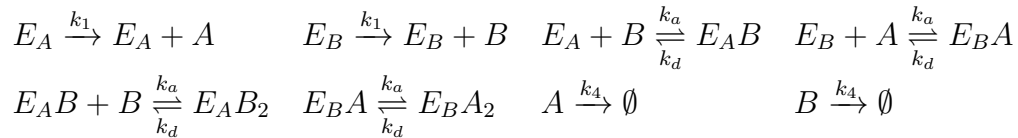


Table 6.2: The chemical reactions of the bi-stable model. The constants take the values $k_1 = 150s^{-1}$, $k_a = 1.2 \times 10^8 s^{-1} M^{-1}$, $k_d = 10s^{-1}$ and $k_4 = 6s^{-1}$.

We have used an implementation of the NSM [10], with support for unstructured meshes added by us. The code is written in C, and wrapped in a MATLAB mex-file. This approach makes the definition of the geometry, the meshing and

the matrix assembly convenient.

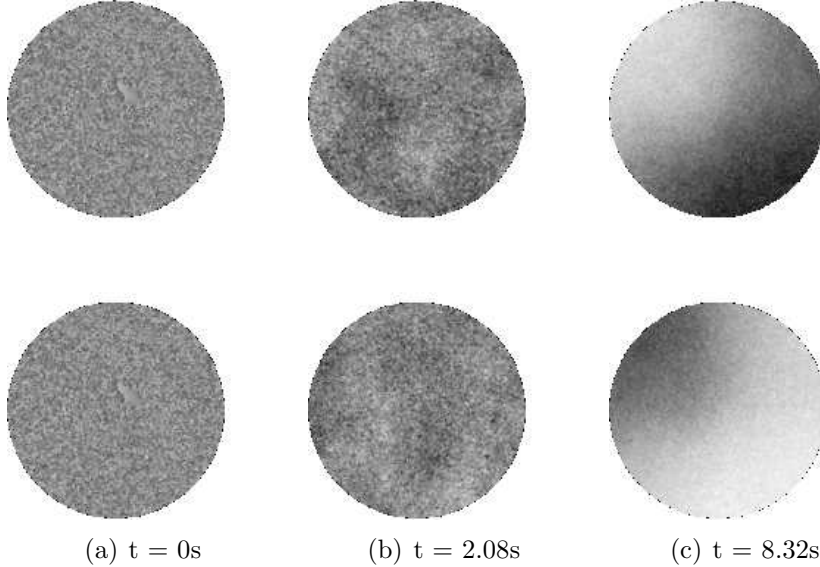


Figure 6.2: Snapshots of the time evolution of one trajectory with diffusion coefficient $\gamma = 2 \times 10^{-13} m^2/s$. The concentrations of the species A and B are found in the upper and lower rows, respectively. Dark areas indicate regions with a higher concentration. Patches with the system in different phases are formed at $t = 8.32s$.

The unstructured mesh has $K = 8849$ nodes, giving a minimal dual cell area of $8.13 \times 10^{-16} m^2$. The mesh quality is not perfect; a few off diagonal elements in the stiffness matrix fail to be non-negative, giving slightly wrong diffusion rates locally. This, however, does not seem to have any profound impact on the behavior of the simulated system when compared to simulations on structured triangular meshes where all coefficients are of the correct sign. The boundaries are reflecting, corresponding to a Neumann boundary condition in the finite element formulation of the macroscopic equation.

The time evolution of the system is simulated on a circle with radius $3 \times 10^{-6} m$ in Figure 6.2 with $\gamma = 2 \times 10^{-13} m^2/s$. There is a domain separation with many A molecules in the lower right part and many B molecules in the upper left part.

In Figure 6.3 the same system is simulated with fast diffusion, $\gamma = 1 \times 10^{-12} m^2/s$, and in this case the system does not separate into domains with different phases. At the end time of this simulation, the system is in a state where A molecules dominate, and the system behaves much like in the homogeneous case.

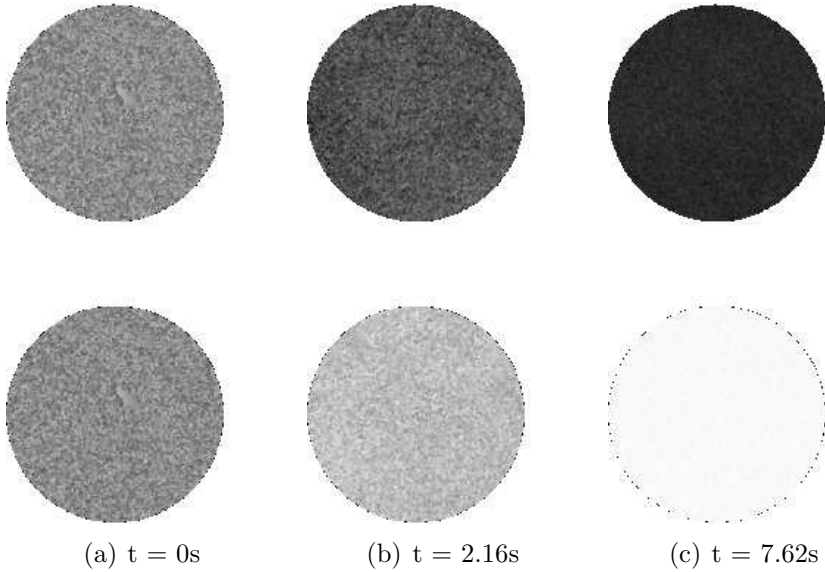


Figure 6.3: The same system as in Figure 6.2 is simulated with $\gamma = 1 \times 10^{-12} m^2/s$. Here the system has not separated into domains with different phases.

6.3 The hybrid method – metabolites and enzymes

A model of a biochemical network with two metabolites A and B and two enzymes E_A and E_B from [40] is simulated in this example. The domain Ω is a disc with radius $\rho_{max} = \pi^{-1/2} \approx 0.564$ and area $|\Omega| = 1$. The reactions are summarized in Table 6.3. Initially, the concentrations a and b are constant and the enzyme concentrations, e_A and e_B , are zero in every cell.

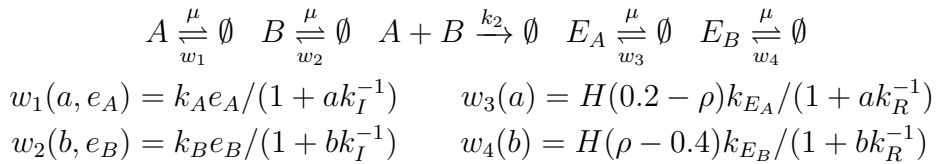


Table 6.3: Reaction channels for the network. The concentrations of the species A, B, E_A , and E_B in a cell are a, b, e_A, e_B . The reaction constants are $k_A = k_B = 3\zeta$, $\mu = 0.002\zeta$, $k_2 = 0.0005\zeta^2$, $k_{E_A} = k_{E_B} = 0.5\zeta$, $k_I = 60/\zeta$, $k_R = 30/\zeta$ and the diffusion constant is $\gamma = 10^{-4}$. The domain is covered by $K = 80$ dual cells and the scaling with the average size of a cell $\zeta \equiv |\Omega|/K$ is done to define the unit scale of the problem. H denotes the Heaviside function; the enzyme E_A is thus produced only in the center of Ω , $0 \leq \rho < 0.2$, and E_B is created only close to the boundary, $0.4 \leq \rho \leq \rho_{max}$.

The chemical reactions and the diffusion of the enzymes are simulated with SSA and the diffusion of A and B is modeled by the diffusion PDE in a straightforward MATLAB implementation of the hybrid method. The effect of the enzymes in different parts of Ω is demonstrated in Figure 6.4 with $M = 10^4$ realizations.

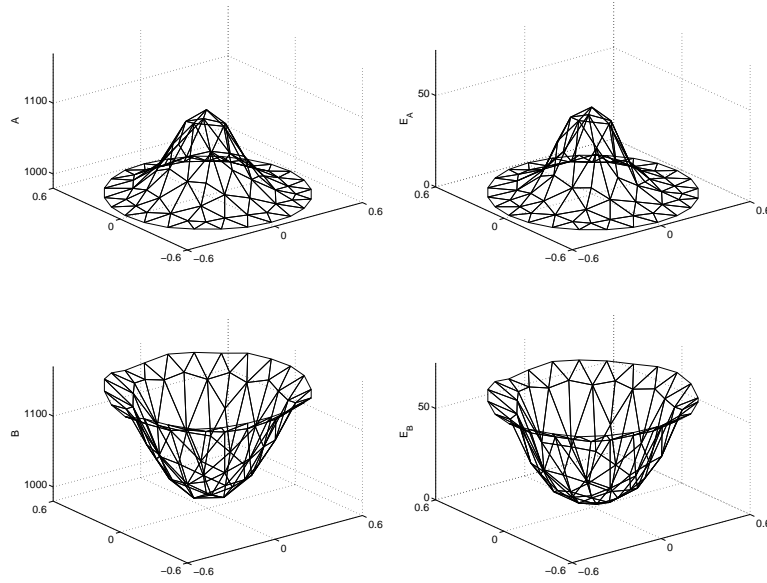


Figure 6.4: The concentrations of the metabolites A (upper left) and B (lower left) and enzymes E_A (upper right) and E_B (lower right) at $t = 200$.

A stochastic reference solution ϕ_i^s , $i = 1, 2, 3, 4$, averaged over $M = 10^4$ trajectories is integrated directly to $t = 200$ with SSA. Hybrid solutions $\phi_i^{\Delta t}(200)$ are computed for different Δt with $M = 10^4$ for comparison with ϕ_i^s . Table 6.4 displays the differences between the stochastic and the hybrid solutions.

Δt	0.1	1	5	20	40	100
δ_t	0.024	0.024	0.024	0.024	0.025	0.030

Table 6.4: The difference between the stochastic solution and the hybrid solution in the ℓ_2 -norm, $\delta_t = \max_i \|\phi_i^s - \phi_i^{\Delta t}\|_2 / (\max_j \phi_{ij}^s - \min_j \phi_{ij}^s)$ at $t = 200$ for different Δt . The stochastic errors dominate in δ_t for $\Delta t \lesssim 40$.

The computational work for the stochastic and the deterministic parts of the algorithm is compared in Figure 6.5 (a) at $t = 200$ with $\gamma = 10^{-4}$ and $M = 10^4$. The work in the deterministic part is less than the work in the stochastic part when $\Delta t > 1$, and decreases as Δt^{-1} when Δt increases. The work for the stochastic part tends to a limit since the extra effort for restarting SSA in each step becomes negligible when the time step is longer.

Figure 6.5 (b) displays the total CPU-time for stochastic and hybrid solutions for different diffusion coefficients γ at $t = 10$ with $M = 10^3$. We use $\Delta t = 5$ for

the hybrid algorithm, i.e. a time step well below the upper limit for which the stochastic errors dominate for $\gamma = 10^{-4}$. The stochastic solutions are integrated directly to $t = 10$. When the diffusion of the molecules is the major part of the computational work for larger $\gamma \gtrsim 10^{-5}$, then replacing the diffusion for the species with large copy numbers by the macroscopic diffusion reduces the CPU-time by up to 1000 while retaining small differences between the solutions, see Table 6.4. The number of molecules of the enzymes $n_e = (\mathbf{x}_3 + \mathbf{x}_4)\mathbf{e}_1$ is about 0.001 of the number of metabolite molecules $n_m = (\mathbf{x}_1 + \mathbf{x}_2)\mathbf{e}_1$ at $t = 10$. This difference explains the remarkable improvement in efficiency in diffusion dominated regimes. From the figure and the discussion, the CPU-times T_{SSA} and T_{hyb} for SSA and the hybrid method, respectively, are approximately

$$T_{SSA} \approx c_{s0} + c_s \gamma (n_m + n_e), \quad T_{hyb} \approx c_{h0} + c_s \gamma n_e,$$

where c_{s0} and c_{h0} are small and are mainly due to the chemical reactions. The concentration of the enzymes increases when the integration is continued to $t = 200$. The speedup by the hybrid method with $\Delta t = 5$ is then about 35. Since $n_m/n_e \approx 30$ this is in agreement with the estimates of T_{SSA} and T_{hyb} above.

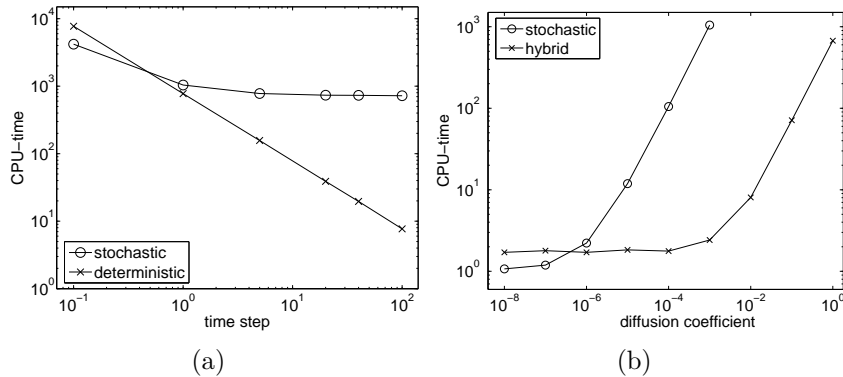


Figure 6.5: Run times versus the time step for the stochastic and deterministic part of the hybrid algorithm (a) and run times versus the diffusion coefficient γ for SSA and the hybrid algorithm (b).

7 Conclusions

The RDME is discretized on an unstructured mesh for better geometric flexibility than a Cartesian mesh. The diffusion coefficients in the RDME are derived from a FEM discretization of the Laplacian. Stochastic simulation can then be used to determine a number of trajectories of the mesoscopic system. If the copy number is large for some chemical species, then a hybrid method integrating the diffusion part deterministically reduces the computing time substantially, especially when the diffusion constant is large.

The method is applied to three different systems. The convergence of a system without reactions to the macroscopic solution is shown in the first example. In the second example, we consider a biochemical system with both diffusion and reactions. We illustrate that our method can be efficiently applied to a previously studied bi-stable system, and that the results obtained with our code are in line with those computed on structured meshes with the freely available software MesoRD [23]. In a final example, the performance of the hybrid method is compared to SSA for a system with four species. The hybrid algorithm is up to three orders of magnitude faster.

In this paper we have considered examples in two space dimensions only. Realistic modeling of the reaction networks in e.g. bacteria typically require 3D simulations. With our approach, the extension to 3D is straightforward and will be reported in a forthcoming paper. The method relies on the FEM discretization of the diffusion equation and a variety of existing software can be used to specify the geometry, construct the mesh and postprocess the result. Presently, we handle diffusion with a uniform diffusion constant but there is no complication in considering space-dependent diffusion or adding convection or to let the diffusion be different for different species.

In the spatially homogeneous case, stiffness arises from the presence of fast chemical reactions. For the RDME, the stiffness in addition increases with the resolution of the mesh. We have proposed a hybrid method to reduce simulation time when some species are present in large copy numbers. For the homogeneous case, many approximative schemes have been developed for systems with time scale separation. For spatially dependent systems, no sharp separation in slow and fast events can generally be made. Instead we rather have a continuum of scales and multiscale simulation techniques have to be developed anew.

References

- [1] S. S. Andrews and D. Bray. Stochastic simulation of chemical reactions with spatial resolution and single molecule detail. *Phys. Biol.*, 1:137–151, 2004.
- [2] O. G. Berg and P. H. von Hippel. Diffusion-controlled macromolecular interactions. *Ann. Rev. Biophys. Chem.*, 14:131–160, 1985.
- [3] D. Bernstein. Simulating mesoscopic reaction-diffusion systems using the Gillespie algorithm. *Phys. Rev. E*, 71:041103, 2005.
- [4] A. N. Borodin and P. Salminen. *Handbook of Brownian Motion*. Birkhauser, Basel, 2002.
- [5] J. Brandts, S. Korotov, M. Křížek, and J. Šolc. On nonobtuse simplicial partitions. *SIAM Review*, 2008. to appear.

- [6] Y. Cao, D. Gillespie, and L. Petzold. Multiscale stochastic simulation algorithm with stochastic partial equilibrium assumption for chemically reacting systems. *J. Comput. Phys.*, 206:395–411, 2005. doi:10.1016/j.jcp.2004.12.014.
- [7] M. Dobrzyński, J. V. Rodríguez, J. A. Kaandorp, and J. G. Blom. Computational methods for diffusion-influenced biochemical reactions. *Bioinformatics*, 23:1969–1977, 2007.
- [8] K. Doubrovinski and M. Howard. Stochastic model for Soj relocation dynamics in *Bacillus subtilis*. *Proc. Natl. Acad. Sci. USA*, 102:9808–9813, 2005.
- [9] W. E, D. Liu, and E. Vanden-Eijnden. Nested stochastic simulation algorithm for chemical kinetic systems with disparate rates. *J. Chem. Phys.*, 123(19):194107, 2005. doi:10.1063/1.2109987.
- [10] J. Elf and M. Ehrenberg. Spontaneous separation of bi-stable biochemical systems into spatial domains of opposite phases. *Syst. Biol.*, 1:230–236, 2004.
- [11] M. B. Elowitz, A. J. Levine, E. D. Siggia, and P. S. Swain. Stochastic gene expression in a single cell. *Science*, 297:1183–1186, 2002.
- [12] S. Engblom. Computing the moments of high dimensional solutions of the master equation. *Appl. Math. Comput.*, 180(2):498–515, 2006. doi:10.1016/j.amc.2005.12.032.
- [13] R. Eymard, T. Gallouët, and R. Herbin. A cell-centred finite-volume approximation for anisotropic diffusion operators on unstructured meshes in any space dimension. *IMA J. Numer. Anal.*, 26:326–353, 2006.
- [14] D. Fange and J. Elf. Noise-induced min phenotypes in *E. coli*. *PLoS Comput. Biol.*, 2:637–648, 2006.
- [15] L. Ferm, P. Lötstedt, and A. Hellander. A hierarchy of approximations of the master equation scaled by a size parameter. *J. Sci. Comput.*, 34:127–151, 2008.
- [16] C. W. Gardiner. *Handbook of Stochastic Methods*. Springer Series in Synergetics. Springer-Verlag, Berlin, 3rd edition, 2004.
- [17] P. L. George. Automatic mesh generation and finite element computation. In P. G. Ciarlet and J. L. Lions, editors, *Handbook of Numerical Analysis*, volume IV, pages 149–190. Elsevier, 1996.
- [18] M. A. Gibson and J. Bruck. Efficient exact stochastic simulation of chemical systems with many species and many channels. *J. Phys. Chem.*, 104(9):1876–1889, 2000. doi:10.1021/jp993732q.

- [19] D. T. Gillespie. A general method for numerically simulating the stochastic time evolution of coupled chemical reactions. *J. Comput. Phys.*, 22(4):403–434, 1976. doi:10.1016/0021-9991(76)90041-3.
- [20] A. Greenbaum. *Iterative Methods for Solving Linear Systems*. SIAM, Philadelphia, 1997.
- [21] P. Guptasarama. Does replication-induced transcription regulate synthesis of the myriad low copy number proteins of *Escherichia coli*? *Bioessays*, 17(11):987–997, 1995. doi:10.1002/bies.950171112.
- [22] E. L. Haseltine and J. B. Rawlings. Approximate simulation of coupled fast and slow reactions for stochastic chemical kinetics. *J. Chem. Phys.*, 117(15):6959–6969, 2002. doi:10.1063/1.1505860.
- [23] J. Hattne, D. Fange, and J. Elf. Stochastic reaction-diffusion simulation with MesoRD. *Bioinformatics*, 21:2923–2924, 2005.
- [24] A. Hellander and P. Lötstedt. A hybrid method for the chemical master equation. *J. Comput. Phys.*, 227:100–122, 2007.
- [25] F. Hermeline. A finite volume method for the approximation of diffusion operators on distorted meshes. *J. Comput. Phys.*, 160:481–499, 2000.
- [26] S. A. Isaacson and C. S. Peskin. Incorporating diffusion in complex geometries into stochastic chemical kinetics simulations. *SIAM J. Sci. Comput.*, 28:47–74, 2006.
- [27] N. G. van Kampen. *Stochastic Processes in Physics and Chemistry*. Elsevier, Amsterdam, 5th edition, 2004.
- [28] K. Kruse and J. Elf. Kinetics in spatially extended systems. In Z. Szallasi, J. Stelling, and V. Periwal, editors, *System Modeling in Cellular Biology. From Concepts to Nuts and Bolts*, pages 177–198. MIT Press, Cambridge, MA, 2006.
- [29] D. Longo and J. Hastay. Dynamics of single-cell gene expression. *Mol. Syst. Biol.*, 2:64, 2006.
- [30] M. Malek-Mansour and J. Houard. A new approximation scheme for the study of fluctuations in nonuniform nonequilibrium systems. *Phys. Lett.*, 70A:366–368, 1979.
- [31] The Mathworks Inc., Natick, MA, USA. *Partial Differential Equation Toolbox 1.0.12*. <http://www.mathworks.com/products/pde>.

- [32] H. H. McAdams and A. Arkin. It's a noisy business. genetic regulation at the nanomolar scale. *Trends Gen.*, 15:65–69, 1999.
- [33] R. Metzler. The future is noisy: The role of spatial fluctuations in genetic switching. *Phys. Rev. Lett.*, 87:068103, 2001.
- [34] W. J. Morokoff and R. E. Caflisch. A quasi-Monte Carlo approach to particle simulation of the heat equation. *SIAM J. Numer. Anal.*, 30:1558–1573, 1993.
- [35] Y.-Y. Nie and V. Thomée. A lumped mass finite-element method with quadrature for a non-linear parabolic problem. *IMA J. Numer. Anal.*, 5:371–396, 1985.
- [36] J. Paulsson, O. G. Berg, and M. Ehrenberg. Stochastic focusing: Fluctuation-enhanced sensitivity of intracellular regulation. *Proc. Natl. Acad. Sci. USA*, 97:7148–7153, 2000.
- [37] T. Poinsoot and D. Veynante. *Theoretical and Numerical Combustion*. Edwards, Philadelphia, PA, 2nd edition, 2005.
- [38] J. M. Raser and E. K. O'Shea. Noise in gene expression: Origins, consequences and control. *Science*, 309:2010–2013, 2005.
- [39] J. V. Rodríguez, J. A. Kaandorp, M. Dobrzyński, and J. G. Blom. Spatial stochastic modelling of the phosphoenolpyruvate-dependent phosphotransferase (pts) pathway in *Escherichia coli*. *Bioinformatics*, 23:1969–1977, 2007.
- [40] P. Sjöberg, P. Lötstedt, and J. Elf. Fokker-Planck approximation of the master equation. *Comput. Visual. Sci.*, 2008. To appear, doi:10.1007/s00791-006-0045-6.
- [41] G. Strang. On the construction and comparison of difference schemes. *SIAM J. Numer. Anal.*, 5:506–517, 1968.
- [42] A. B. Stundzia and C. L. Lumsden. Stochastic simulation of coupled reaction-diffusion processes. *J. Comput. Phys.*, 127:196–207, 1996.
- [43] M. Svärd, J. Gong, and J. Nordström. An accuracy evaluation of unstructured node-centred finite volume methods. *Appl. Numer. Math.*, 2008. in press.
- [44] V. Thomée. *Galerkin Finite Element Methods for Parabolic Problems*. Springer, Berlin, 1997.
- [45] V. Thomée and L. Wahlbin. On the existence of maximum principles in parabolic finite element equations. *Math. Comp.*, 77:11–19, 2008.

- [46] J. Xu and L. Zikatanov. A monotone finite element scheme for convection-diffusion equations. *Math. Comp.*, 68:1429–1446, 1999.
- [47] J. S. van Zon and P. Rein ten Wolde. Green’s-function reaction dynamics: A particle-based approach for simulating biochemical networks in time and space. *J. Chem. Phys.*, 123:234910, 2005.
- [48] B. Øksendal. *Stochastic Differential Equations*. Springer-Verlag, New York, 2005.